
Representation Learning on Heterophilic Graph with Directional Neighborhood Attention

Qincheng Lu¹ Jiaqi Zhu¹ Sitao Luan^{†12} Xiao-Wen Chang^{†1}

Abstract

Graph Attention Network (GAT) is one of the most popular Graph Neural Network (GNN) architecture, which employs the attention mechanism to learn edge weights and has demonstrated promising performance in various applications. However, since it only incorporates information from immediate neighborhood, it lacks the ability to capture long-range and global graph information, leading to unsatisfactory performance on some datasets, particularly on heterophilic graphs. To address this limitation, we propose the Directional Graph Attention Network (DGAT) in this paper. DGAT is able to combine the feature-based attention with the global directional information extracted from the graph topology. To this end, a new class of Laplacian matrices is proposed which can provably reduce the diffusion distance between nodes. Based on the new Laplacian, topology-guided neighbour pruning and edge adding mechanisms are proposed to remove the noisy and capture the helpful long-range neighborhood information. Besides, a global directional attention is designed to enable a topological-aware information propagation. The superiority of the proposed DGAT over the baseline GAT has also been verified through experiments on real-world benchmarks and synthetic data sets. It also outperforms the state-of-the-art (SOTA) models on 6 out of 7 real-world benchmark datasets.

1. Introduction

Combining graph signal processing and Convolutional Neural Networks (CNNs) (LeCun et al., 1998), Graph Neural Networks (GNNs) has achieved remarkable results on ma-

chine learning tasks with non-Euclidean data (Scarselli et al., 2008; Kipf & Welling, 2016; Hamilton et al., 2017; Velickovic et al., 2017; Xu et al., 2018; Luan et al., 2019; Beaini et al., 2021; Zhao et al., 2021; Hua et al., 2023). Unlike CNNs where neighbours are weighted differently, the convolutional kernel in the vanilla GNNs (Kipf & Welling, 2016) and many other popular variants (Hamilton et al., 2017; Xu et al., 2018) assign the same weight in a neighbourhood. The Graph Attention Network (GAT) (Velickovic et al., 2017) overcomes this limitation by allowing nodes to connect to its local neighbours with learnable weights.

The GAT model generates the node representation solely based on the representations of its direct neighbours and this works well on the homophilic graphs (Luan et al., 2023a), where the node and its neighbours are likely to have the same label. However, GAT suffers from significant performance loss in node classification tasks involving heterophilic graphs (Zhu et al., 2020; Luan et al., 2022b), where nodes from different classes tend to be connected.

Non-local neighborhood information is found to be helpful to deal with heterophily problem for GNNs (Abu-El-Haija et al., 2019; Liu et al., 2020; Zhu et al., 2020; He et al., 2021; Zheng et al., 2022), but it has not been leveraged in GAT model and we will address this issue in this paper. The main contribution of our paper is: (1) We propose a new class of parameterized normalized graph Laplacian matrices which have better control over directional aggregation and can contain the widely used normalized Laplacians as special cases. Through the parameters in new Laplacian, we can adjust the diffusion distances and spectral distances between nodes by altering the spectral property of the graph; (2) We establish a theorem that enables the usage of the spectral distance as a surrogate function of diffusion distance, which significantly reduce the computational cost for comparing the relative distance between nodes. It substantially extends the scope and overcomes some shortcomings of (Beaini et al., 2021). (3) Based on the new graph Laplacian, we propose the Directional Graph Attention Network (DGAT). The contributions of DGAT are two folds: i. a topology-guided graph rewiring strategy with theoretical justifications; ii. a global directional attention which enables a topological-aware information propagation. The empirical results demonstrate the effectiveness and superiority of DGAT compared with

[†]Corresponding author ¹McGill University ²Mila - Quebec Artificial Intelligence Institute. Correspondence to: Sitao Luan <sitao.luan@mail.mcgill.ca>, Xiao-Wen Chang <chang@cs.mcgill.ca>.

SOTA GNNs for node classification tasks on graph across various homophily levels. The proposed strategy is characterized by flexibility and seamless integration with the original GAT architecture and other types of graph attention mechanism.

This paper will be organized as follows: notation and background knowledge are introduced in Section 2; in Section 3, we propose the new class of Laplacian, show its properties, prove the theoretical results on spectral and diffusion distances and put forward the DGAT architecture; in Section 4, we discuss related works; in Section 5, we show the experimental results and comparisons on synthetic and real-world graphs.

2. Preliminaries

In this section, we introduce notation and background knowledge. We use **bold** font for vectors and matrices. For a matrix $\mathbf{B} = (b_{ij})$, $|\mathbf{B}| = (|b_{ij}|)$ and its i^{th} row is denoted as $\mathbf{B}_{i,:}$ or \mathbf{b}_i^{T} . We use $\mathbf{B}||\mathbf{C}$ and $[\mathbf{B}, \mathbf{C}]$ to denote column and row concatenation of matrices \mathbf{B} and \mathbf{C} , respectively. We use $\mathcal{G} = (\mathcal{V}, \mathcal{E})$ to denote an undirected connected graph with the vertex set \mathcal{V} (with $|\mathcal{V}| = N$) and the edge set \mathcal{E} . We have a node feature matrix $\mathbf{X} \in \mathbb{R}^{N \times d_0}$ whose i^{th} row is the transpose of the feature vector $\mathbf{x}_i \in \mathbb{R}^{d_0}$ of node v_i . The learned node representation matrix at the l^{th} layer of GNNs is denoted by $\mathbf{H}^{(l)} \in \mathbb{R}^{N \times d_l}$. For a node $v_i \in \mathcal{V}$, $\mathcal{N}(v_i) \subseteq \mathcal{V}$ denotes the set of neighbouring nodes of v_i . The adjacency matrix of \mathcal{G} is denoted by $\mathbf{A} = (a_{ij}) \in \mathbb{R}^{N \times N}$ with $a_{ij} = 1$ if $e_{ij} \in \mathcal{E}$ and $a_{ij} = 0$ otherwise. The degree matrix of \mathcal{G} is $\mathbf{D} = \text{diag}(d_{ii}) \in \mathbb{R}^{N \times N}$ with $d_{ii} = \sum_j a_{ij}$. Three Laplacian matrices, namely the combinatorial Laplacian, random-walk normalized Laplacian and symmetric normalized Laplacian are respectively defined as:

$$\mathbf{L} = \mathbf{D} - \mathbf{A}, \quad \mathbf{L}_{\text{rw}} = \mathbf{D}^{-1}\mathbf{L}, \quad \mathbf{L}_{\text{sym}} = \mathbf{D}^{-\frac{1}{2}}\mathbf{L}\mathbf{D}^{-\frac{1}{2}}. \quad (1)$$

We use $\phi^{(k)}$ to denote the k^{th} eigenvector of a Laplacian corresponding to the k^{th} smallest positive eigenvalue $\lambda^{(k)}$.

2.1. Graph Neural Networks

Most modern GNNs adopt the message-passing framework (Hamilton, 2020), in which the representation \mathbf{h}_u of node u is generated by iterative aggregation of its neighbourhood representations and its own representation generated from the previous layer. The l^{th} layer of a GNN can be represented by the two following operations (Hamilton, 2020):

$$\begin{aligned} \mathbf{m}_u^{(l)} &= \text{AGGREGATE}^{(l)}(\{\mathbf{h}_v^{(l-1)} : \forall v \in \mathcal{N}(u)\}), \\ \mathbf{h}_u^{(l)} &= \text{UPDATE}^{(l)}(\mathbf{h}_u^{(l-1)}, \mathbf{m}_u^{(l)}), \end{aligned} \quad (2)$$

where $\mathbf{m}_u^{(l)}$ is the aggregated message by applying the AGGREGATE operator to node u 's direct neighbours; and

$\mathbf{h}_u^{(l)}$ is the representation for node u in the l^{th} layer generated by the UPDATE operator.

2.2. Graph Attention Mechanism

The graph attention is defined as a function $g : u \times \mathcal{N}(u) \rightarrow [0, 1]$ that maps the node u and any node in $\mathcal{N}(u)$ to a relevance score (Lee et al., 2019). For example, $r_{ij}^{(l)}$, the attention score that node v_i gives to node v_j at the l^{th} layer can be defined as

$$r_{ij}^{(l)} = \text{LeakyReLU}((\mathbf{a}^{(l)})^{\text{T}}[\mathbf{W}^{(l)}\mathbf{h}_i^{(l-1)}||\mathbf{W}^{(l)}\mathbf{h}_j^{(l-1)}]). \quad (3)$$

where $\mathbf{a}^{(l)} \in \mathbb{R}^{2d_l}$ and $\mathbf{W}^{(l)} \in \mathbb{R}^{d_l \times d_{l-1}}$ are learnable parameters. Denote $\mathbf{R}^{(l)} = (r_{ij}^{(l)}) \in \mathbb{R}^{N \times N}$. Then GAT uses a mask matrix $\mathbf{M} = (m_{ij}) \in \mathbb{R}^{N \times N}$ to preserve the structural information and normalize the attention score:

$$\begin{aligned} \alpha_{ij}^{(l)} &= \text{softmax}_j(\tilde{\mathbf{R}}_{i,:}^{(l)}), \quad \tilde{\mathbf{R}}^{(l)} = \mathbf{R}^{(l)} + \mathbf{M}, \\ m_{ij} &= \begin{cases} 0, & e_{ij} \in \mathcal{E} \\ -\infty, & \text{otherwise} \end{cases}. \end{aligned} \quad (4)$$

The representation $\mathbf{h}_i^{(l)}$ for node v_i at the l^{th} layer is calculated as follows:

$$\begin{aligned} \mathbf{m}_i^{(l)} &= \sum_{j:v_j \in \{\mathcal{N}(v_i)\}} \alpha_{ij}^{(l)} \mathbf{W}^{(l)} \mathbf{h}_j^{(l-1)}, \\ \mathbf{h}_i^{(l)} &= \sigma(\mathbf{m}_i^{(l)} + \alpha_{ii}^{(l)} \mathbf{W}^{(l)} \mathbf{h}_i^{(l-1)}), \end{aligned} \quad (5)$$

where $\sigma(\cdot)$ is a non-linear activation function.

2.3. Directional Aggregation Operators

Directional Graph Network (DGN) (Beaini et al., 2021) is proposed to distinguish messages from neighbours with different topological importance. DGN explicitly assigns different weights to nodes within a neighbourhood directional using two aggregation matrix, namely the directional average matrix \mathbf{B}_{av} and the directional derivative matrix \mathbf{B}_{dx} defined as follows:¹:

$$\mathbf{B}_{\text{av}}(\phi) = |\nabla\phi|, \quad \mathbf{B}_{\text{dx}}(\phi) = \nabla\phi - \text{diag}(\nabla\phi\mathbf{1}), \quad (6)$$

where $\nabla\phi = (\nabla\phi_{ij}) \in \mathbb{R}^{N \times N}$ is the graph vector field of a graph signal $\phi = (\phi_i) \in \mathbb{R}^N$ defined as follows:

$$\nabla\phi_{ij} = \begin{cases} \phi_j - \phi_i, & e_{ij} \in \mathcal{E} \\ 0, & \text{otherwise} \end{cases}. \quad (7)$$

In (Beaini et al., 2021), ϕ is taken to be $\phi^{(1)}$, the eigenvector corresponding to the smallest positive eigenvalue

¹In practice, row-normalized $\widetilde{\nabla\phi}$ is used instead where $\widetilde{\nabla\phi}_{i,:} = \frac{\nabla\phi_{i,:}}{\|\nabla\phi_{i,:}\|_1 + \epsilon_0}$ with a small positive number ϵ_0 .

of \mathbf{L}_{rw} . Note that $\nabla\phi^{(1)}$ is the dominant direction of the graph diffusion process (Nadler et al., 2005). For message passing, DGN regards the \mathbf{B}_{av} and \mathbf{B}_{dx} as edge weights for aggregation:

$$\begin{aligned} \mathbf{m}_i^{(l)} &= \sum_{j:v_j \in \mathcal{N}(v_i)} \mathbf{W}^{(l)} [(\mathbf{B}_{\text{av}}(\phi^{(1)}))_{ij} \mathbf{h}_j^{(l-1)} \| (\mathbf{B}_{\text{dx}}(\phi^{(1)}))_{ij} \mathbf{h}_j^{(l-1)}], \\ \mathbf{h}_i^{(l)} &= \text{MLP} \left([\mathbf{m}_i^{(l)} \| \mathbf{h}_i^{(l-1)}] \right). \end{aligned} \quad (8)$$

The authors in (Beaini et al., 2021) claim that \mathbf{B}_{av} and \mathbf{B}_{dx} indicate a direction that can reduce diffusion distance. And we refer to the operation $\mathbf{B}_{\{\text{av}, \text{dx}\}}(\phi^{(1)})\mathbf{H}$ as the directional aggregation.

2.4. Spectral-based Nodes Relative Distances

The relative position of nodes on the graph could be told by eigenvectors of Laplacian matrices (Kreuzer et al., 2021). As the graph data is non-Euclidean, various measurements are proposed to describe the distance between nodes (Nadler et al., 2005; Qiu & Hancock, 2007; Belkin & Niyogi, 2003). Among them, the diffusion distance is often used to model how node v_i influence node v_j by considering random walks along edges (Beaini et al., 2021). At the initial step, the random walk start at a node, and moves to one of its neighbours at the next step. The diffusion distance between v_i and v_j is proportional to the probability that the random walk starting at node v_i meets the random walk starting at node v_j at step t . Based on \mathbf{L}_{rw} , the **diffusion distance** is calculated as (see (Coifman & Lafon, 2006)):

$$d_t(v_i, v_j; \mathbf{L}_{\text{rw}}) = \left(\sum_{k=1}^{n-1} e^{-2t\lambda^{(k)}} (\phi_i^{(k)} - \phi_j^{(k)})^2 \right)^{\frac{1}{2}}. \quad (9)$$

Another measure of the distance between v_i and v_j is the **spectral distance** defined as (see (Belkin & Niyogi, 2003)):

$$d_s(v_i, v_j; \mathbf{L}_{\text{rw}}) = |\phi_i^{(1)} - \phi_j^{(1)}|. \quad (10)$$

Note that $\phi^{(1)}$ gives positional information of nodes (Dwivedi & Bresson, 2020; Kreuzer et al., 2021; Muller et al., 2023) and $\mathbf{B}_{\text{av}}(\phi^{(1)}) = (d_s(v_i, v_j; \mathbf{L}_{\text{rw}}))$. A more general definition of d_s involves the k eigenvectors corresponding to the k smallest eigenvalues, but here we take $k = 1$ for simplicity and informativeness.

2.5. Homophily Metrics

In the context of graph representation learning, homophily refers to the tendency for nodes in a graph to share the same labels with their neighbours (McPherson et al., 2001). Heterophily, conversely, describes the tendency for nodes to connect with other nodes with different labels. In this study, we employ the node homophily metric $H_{\text{node}} \in [0, 1]$

defined as (see (Pei et al., 2020)²):

$$H_{\text{node}} = \frac{1}{|\mathcal{V}|} \sum_{u \in \mathcal{V}} \frac{|y_u = y_v : v \in \mathcal{N}(u)|}{|\mathcal{N}(u)|}. \quad (11)$$

Graphs with strong homophily have large H_{node} (typically between 0.5 and 1); on the contrary, heterophilic graphs have small H_{node} (typically < 0.5). Various alternative metrics including edge homophily (Zhu et al., 2020), class homophily (Lim et al., 2021), aggregation homophily (Luan et al., 2022a), graph smoothness value (Luan et al., 2023a) and classifier-based performance metrics (Luan et al., 2023b) can also be used in practice.

3. The Directional Attention Mechanism

In this section, we propose Directional Graph Attention Network (DGAT), which aims to enhance the graph attention mechanism to capture long-range neighborhood information on graphs with different homophily levels, especially on heterophilic graphs. In Section 3.1, we first propose a new parameterized normalized Laplacian matrix, which defines a new class of Graph Laplacian with more general directional aggregation. We then elaborate on the global directional flow in DGAT, which is defined based on the vector field utilizing the low-frequency eigenvector of this new class of Laplacian matrices. More specifically, two new mechanisms are introduced: the topology-guided neighbour rewiring (Section 3.2 and Section 3.3) and the global directional attention (Section 3.4). Finally, we summarize the architecture of DGAT in Section 3.5.

3.1. Parameterized Normalized Laplacian

In order to gain a more refined control over the directional aggregation, we define a new class of Laplacian matrices.

Definition 3.1. A parameterized normalized Laplacian matrix is defined as

$$\mathbf{L}^{(\alpha, \gamma)} = \gamma[\gamma\mathbf{D} + (1 - \gamma)\mathbf{I}]^{-\alpha} \mathbf{L} [\gamma\mathbf{D} + (1 - \gamma)\mathbf{I}]^{\alpha-1} \quad (12)$$

and the corresponding parameterized normalized adjacent matrix is defined as

$$\mathbf{P}^{(\alpha, \gamma)} = \mathbf{I} - \mathbf{L}^{(\alpha, \gamma)}, \quad (13)$$

where the parameters $\gamma \in (0, 1]$ and $\alpha \in [0, 1]$.

The normalized Laplacian matrices defined in Eq. (1) are special cases of this new class of Laplacian matrices: when $\alpha = 1$ and $\gamma = 1$, $\mathbf{L}^{(\alpha, \gamma)} = \mathbf{L}_{\text{rw}}$; when $\alpha = \frac{1}{2}$ and $\gamma = 1$, $\mathbf{L}^{(\alpha, \gamma)} = \mathbf{L}_{\text{sym}}$. Although we cannot choose α and γ such that $\mathbf{L}^{(\alpha, \gamma)}$ becomes \mathbf{L} , we have $\lim_{\gamma \rightarrow 0} \frac{1}{\gamma} \mathbf{L}^{(\alpha, \gamma)} = \mathbf{L}$,

²See more metrics in (Luan et al., 2023b).

which implies that when γ is small enough, an eigenvector of $\mathbf{L}^{(\alpha,\gamma)}$ is a good approximation to an eigenvector of \mathbf{L} .

The following theorem justifies the definition of $\mathbf{P}^{(1,\gamma)}$ as a random walk matrix.

Theorem 3.2. *The $\mathbf{P}^{(\alpha,\gamma)}$ defined in (13) is non-negative (i.e., all of its elements are non-negative), and when $\alpha = 1$, $\mathbf{P}^{(\alpha,\gamma)}\mathbf{1} = \mathbf{1}$. See the proof in Appendix B.1.*

The theorem indicates $\mathbf{P}^{(1,\gamma)}$ is a random walk matrix, which is a generalization of the classic random walk matrix $\mathbf{D}^{-1}\mathbf{A}$. The properties of eigenvalues of $\mathbf{L}^{(\alpha,\gamma)}$ are given in the following Theorem.

Theorem 3.3. *Suppose the graph \mathcal{G} is connected. Then the symmetric $\mathbf{L}^{(1/2,\gamma)} \in \mathbb{R}^{n \times n}$ has the eigendecomposition:*

$$\mathbf{L}^{(1/2,\gamma)} = \mathbf{U}\mathbf{\Lambda}^{(\gamma)}\mathbf{U}^T, \quad (14)$$

where $\mathbf{U} \in \mathbb{R}^{N \times N}$ is orthogonal and $\mathbf{\Lambda}^{(\gamma)} = \text{diag}(\lambda^{(i)}(\gamma))$,

$$0 = \lambda^{(0)}(\gamma) < \lambda^{(1)}(\gamma) \leq \dots \leq \lambda^{(N-1)}(\gamma) \leq 2. \quad (15)$$

Each $\lambda^{(i)}(\gamma)$ is strictly increasing with respect to γ for $i = 1 : N - 1$. Furthermore, $\mathbf{L}^{(\alpha,\gamma)}$ has the eigendecomposition

$$\mathbf{L}^{(\alpha,\gamma)} = \left([\gamma\mathbf{D} + (1-\gamma)\mathbf{I}\right]^{\frac{1}{2}-\alpha}\mathbf{U}\mathbf{\Lambda}^{(\gamma)}\left([\gamma\mathbf{D} + (1-\gamma)\mathbf{I}\right]^{\frac{1}{2}-\alpha}\mathbf{U}\right)^{-1}, \quad (16)$$

i.e., $\mathbf{L}^{(\alpha,\gamma)}$ share the same eigenvalues as $\mathbf{L}^{(1/2,\gamma)}$ and the columns of $[\gamma\mathbf{D} + (1-\gamma)\mathbf{I}]^{\frac{1}{2}-\alpha}\mathbf{U}$ are the corresponding eigenvectors. See proof in Appendix B.2.

The following theorem shows the monotonicity of the diffusion distance with respect to the spectral distance. Here both distances are defined in terms of eigenvectors of $\mathbf{L}^{(1,\gamma)}$, cf. (9) and (10), which involve the eigenvectors of \mathbf{L}_{rw} .

Theorem 3.4. *Let v_i , v_j and v_m be nodes of the graph \mathcal{G} such that $d_s(v_m, v_j; \mathbf{L}^{(1,\gamma)}) < d_s(v_i, v_j; \mathbf{L}^{(1,\gamma)})$. Then there is a constant C such that for $t \geq C$,*

$$d_t(v_m, v_j; \mathbf{L}^{(1,\gamma)}) < d_t(v_i, v_j; \mathbf{L}^{(1,\gamma)}). \quad (17)$$

Furthermore, the ratio $d_t(v_m, v_j; \mathbf{L}^{(1,\gamma)})/d_t(v_i, v_j; \mathbf{L}^{(1,\gamma)})$ is proportional to $e^{-\lambda^{(1)}(\gamma)}$.

Theorem 3.4³ shows that the spectral distance can be used as a good indicator of the diffusion distance, i.e., if node i has a larger spectral distance to node j than node m , then node i would also have a larger diffusion distance to node j after enough time steps. According to (9), we need to

³Theorem 3.4 substantially extends the scope of (Beaini et al., 2021), which deals with the diffusion distance defined by the random walk Laplacian \mathbf{L}_{rw} . Furthermore, Theorem 3.4 overcomes some shortcomings of (Beaini et al., 2021), see details in Appendix B.3.

find all eigenvalues and eigenvectors of the Laplacian to calculate the diffusion distance, which is computationally expensive. But as Theorem 3.4 shows, we can easily compute the spectral distance and use it as a surrogate function of diffusion distance.

For graphs with different homophily levels, the node would prefer neighborhood information from different diffusion distances. Specifically, **nodes with small diffusion distances would be favored on homophilic graphs and nodes with large diffusion distances would be helpful on heterophilic graphs to reduce the effect of noises (Topping et al., 2021)**. Adjusting α and γ can change the eigenvalues and eigenvectors of $\mathbf{L}^{(\alpha,\gamma)}$, leading to adjustment of diffusion distances. For instance, we can employ a smaller γ on heterophilic graphs to help the propagation of long-range neighborhood information and employ a larger γ on homophilic graphs to capture the useful local information. Therefore, we can tune α and γ as hyperparameters to control the message passing in a nuanced way.

3.2. Topology-Guided Neighbour Pruning

In order to filter out the noise, i.e., inter-class information, during feature aggregation, we propose a novel topology-guided neighbour pruning strategy to remove the noisy neighbors.

The diffusion distance can be regarded as a measure of node dependency (Coifman et al., 2005) or a criterion for the efficiency of message passing between nodes that are not directly connected. For connected nodes v_i and v_j , although $d_t(v_i, v_j; \mathbf{L}^{(1,\gamma)})$ may be large, the message from v_j still reaches v_i in one step via e_{ij} in GNNs' message passing.

Based on Theorem 3.4, we propose to use $d_s(v_i, v_j; \mathbf{L}^{(1,\gamma)})$ to determine whether the $v_j \in \mathcal{N}(v_i)$ tends to propagate noisy information to v_i under the homophily and heterophily assumptions, respectively.

Let $\phi^{(1)}$ be the eigenvector of $\mathbf{L}^{(1,\gamma)}$ corresponding to the smallest non-trivial eigenvalue. For node i and its neighbor $v_j \in \mathcal{N}(v_i)$, assume $\phi_j^{(1)}(\gamma) > \phi_i^{(1)}(\gamma)$. For $v_k \notin \mathcal{N}(v_i)$ satisfying the following conditions

$$\phi_k^{(1)}(\gamma) > \phi_i^{(1)}(\gamma), d_t(v_k, v_i; \mathbf{L}^{(1,\gamma)}) > \frac{1}{2}d_t(v_i, v_j; \mathbf{L}^{(1,\gamma)}), \quad (18)$$

we have $d_t(v_k, v_j; \mathbf{L}^{(1,\gamma)}) < d_t(v_k, v_i; \mathbf{L}^{(1,\gamma)})$. This means node v_j (which is connected to node v_i) with smaller diffusion distance are more likely to be used to accelerate message passing from node v_k to node v_i . Based on the above discussion about the condition of v_k should satisfy, we propose the following neighbour pruning strategy to remove neighbors that will carry more higher-order neighborhood information in homophilic graphs and eliminate neighbors which can carry less higher-order information

in heterophilic graphs. With a pre-defined threshold ϵ ⁴, we compare each $d_s(v_i, v_j; \mathbf{L}^{(1, \gamma)})$ against ϵ and decide whether e_{ij} should be pruned regarding the following two cases.

The homophily case It follows that the smaller $d_s(v_i, v_j; \mathbf{L}^{(1, \gamma)})$ is, the larger the set of nodes satisfying the condition in (18) is. Which means that neighbour v_j with smaller $d_s(v_i, v_j; \mathbf{L}^{(1, \gamma)})$ tends to carry more diverse information propagated from nodes with wider range of diffusion distance to v_i . Under the homophily assumption, nodes are more likely to share labels with local neighbours than higher-order neighbors. Thus, GNNs should receive more information from local neighbours $\mathcal{N}(v_i)$ with less potential to carry higher-order neighborhood information. Therefore, edges with $d_s(v_i, v_j; \mathbf{L}^{(1, \gamma)}) < \epsilon$ are pruned, as they introduce more noise which may prohibit graph representation learning on a homophily graph.

The heterophily case Conversely, the larger $d_s(v_i, v_j; \mathbf{L}^{(1, \gamma)})$ is, the more likely that neighbor v_j tends to carry less higher-order information to v_i . Thus edges with $d_s(v_i, v_j; \mathbf{L}^{(1, \gamma)}) > \epsilon$ are pruned.

3.3. Topology-Guided Edge Adding

For heterophilic graphs, edges pruning is not enough. Unlike the neighbor denoising for the heterophily case in Section 3.2, where the edges are assumed to be inter-class, we are going to add intra-class edges to provide extra beneficial information for message propagation under the assumption that disconnected nodes with large diffusion distance are more likely to share labels in a heterophily graph (Topping et al., 2021). However, it tends to bring a large amount of unhelpful edges if we connect every pair of nodes with large diffusion distance. We propose the following strategy to identify the most helpful nodes to add edges on.

Let $\phi_m^{(1)}(\gamma) = \min_k \phi_k^{(1)}(\gamma)$, $\phi_n^{(1)}(\gamma) = \max_k \phi_k^{(1)}(\gamma)$ and $M = \frac{1}{2}(\phi_m^{(1)}(\gamma) + \phi_n^{(1)}(\gamma))$. For each node v_i with $\phi_i^{(1)}(\gamma) < M$, we connect this v_i to v_n . The newly added edge helps propagating information from any unconnected nodes with a large diffusion distance to v_i . To explain it, consider v_j with the property

$$v_j \notin \mathcal{N}(v_i), \quad d_s(v_i, v_j; \mathbf{L}^{(1, \gamma)}) > M, \quad (19)$$

we have $d_t(v_n, v_j; \mathbf{L}^{(1, \gamma)}) < d_t(v_n, v_i; \mathbf{L}^{(1, \gamma)})$.

Then the newly added edge e_{in} makes v_n a useful neighbor of v_i , which promotes message passing from all v_j with a large diffusion distance ($> M$) to v_i .

⁴We treat ϵ as a hyperparameter, and it is tuned independently for different datasets

For each node v_i with $\phi_i^{(1)}(\gamma) > M$, we connect node v_i and node v_m and the reason is similar to that given above.

3.4. Global Directional Attention

The original GAT employs multi-head attention to enrich the model’s capabilities and stabilize the learning process (Velickovic et al., 2017), but each attention head is feature-based and does not adapt to the specific characteristics of the global topology. In contrast, the DGN projects incoming messages into directions defined by the graph topology (Beaini et al., 2021) but utilizes fixed weights within node neighbourhoods, consequently losing flexibility in local aggregation. To remedy these shortcomings, we propose a global directional attention mechanism, which is characterized by spectral-based edge features and topology-aware attention.

3.4.1. SPECTRAL-BASED EDGE FEATURES

We propose to define the feature of $e_{ij} \in \mathcal{E}$ as

$$\mathbf{f}^{(i, j)} = [\mathbf{B}_{\text{av}}(\phi^{(1)}(\gamma))(i, j), \mathbf{B}_{\text{dx}}(\phi^{(1)}(\gamma))(i, j)]^\top, \quad (20)$$

where $\mathbf{B}_{\text{av}}(\phi^{(1)}(\gamma))$ and $\mathbf{B}_{\text{dx}}(\phi^{(1)}(\gamma))$ are matrices corresponding to the aggregation and diversification operations utilizing the vector field $\nabla \phi^{(1)}(\gamma)$ (see (6)). By Theorem 3.4, $\mathbf{B}_{\{\text{av}, \text{dx}}(\phi^{(1)}(\gamma))(i, j)$ contains information of the diffusion distance between v_i and v_j , which describes the relative position of v_i and v_j on the graph. Instead of regarding them as edge weights, we use this node relative distance information to assist the learning of attention between nodes.

3.4.2. TOPOLOGY-AWARE ATTENTION

We propose to define the attention score between v_i and v_j before normalization as:

$$r_{ij}^{(l)} = \text{LeakyReLU}((\mathbf{a}^{(l)})^\top [\mathbf{W}_n^{(l)} \mathbf{h}_i^{(l-1)} \|\mathbf{W}_n^{(l)} \mathbf{h}_j^{(l-1)} \|\mathbf{W}_e^{(l)} \mathbf{f}^{(i, j)}]), \quad (21)$$

where $\mathbf{W}_n^{(l)}$ and $\mathbf{W}_e^{(l)}$ are learnable weights for node representation and edge features respectively. The normalized attention score is calculated according to (4). Compared with GAT, the additional number of parameters in (21) is negligible, since $\mathbf{f}^{(i, j)} \in \mathbb{R}^2$. The normalized attention score ($\alpha_{ij}^{(l)}$) is calculated according to graph connectivity by (4).

3.5. Directional Graph Attention Network

Figure 1 provides a schematic representation of the workflow of DGAT model. Here we use $\alpha = 1$ as an example. Given the graph $\mathcal{G} = (\mathcal{V}, \mathcal{E})$ and the hyperparameter γ , the DGAT calculates the first non-trivial eigenvector $\phi^{(1)}(\gamma)$ of $\mathbf{L}^{(1, \gamma)}$. Based on $\nabla \phi^{(1)}(\gamma)$ and the pruning threshold ϵ , the neighbour pruning or the edge adding strategy is performed,

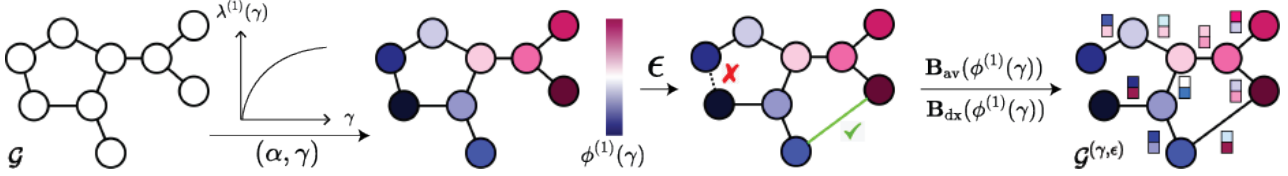


Figure 1. The workflow of DGAT.

and is tailored to either a homophily or heterophily scenario. We denote the rewired graph as $\mathcal{G}^{(\gamma, \epsilon)} = (\mathcal{V}, \mathcal{E}^{(\gamma, \epsilon)})$ with self-loop added to it⁵. Edge features are defined according to (20) based on the pruned graph. Utilizing multi-heads attention (Vaswani et al., 2017; Velickovic et al., 2017), the l^{th} layer of DGAT updates the representation of v_i as

$$\mathbf{h}_i^{(l)} = \left(\left\| \left\| \sigma \left(\sum_{j: e_{ij} \in \mathcal{E}^{(\gamma, \epsilon)}} \alpha_{ij}^{(l, m, \gamma, \epsilon)} \mathbf{W}^{(l, m)} \mathbf{h}_j^{(l-1)} \right) \right\|_{m=1}^M \right) \mathbf{W}^{(l)}, \quad (22)$$

where M is the number of heads, $\alpha_{ij}^{(l, m, \gamma, \epsilon)}$ is the topology-aware attention on m^{th} head defined in Section 3.4.2.

4. Related Works

A general graph shift operator is proposed in (Eliasof et al., 2023) to include various kinds of adjacency and Laplacian matrices. While (Eliasof et al., 2023) propose a learnable graph shift operation. The new class of Laplacians in this work distinguishes from them as its eigenvalues are bounded and offer a theoretical way to control the spectral property of graph.

We have seen methods that enhance GNNs’ performance by changing the graph structure (Rong et al., 2019; Papp et al., 2021). Graph rewiring, including spatial rewiring (Abu-El-Haija et al., 2019) and spectral-based methods (Arnaiz-Rodríguez et al., 2022), are proposed to alleviate over-squashing (Alon & Yahav, 2020). While our method is characterized by its adaptiveness to different heterophily levels.

Several recent studies have incorporated the attention mechanism into GNNs (Brody et al., 2021; Yun et al., 2019; Hu et al., 2020; Wang et al., 2020; Luan et al., 2022a), and research interests in graph transformer are rising (Kreuzer et al., 2021; Muller et al., 2023). In our implementation, we use the graph attention mechanism proposed in GAT (Velickovic et al., 2017). Our proposed method is immune to the specific attention mechanism it can combine with, offering the potential to enhance various graph-based attention mechanisms including graph transformers. Using the vanilla graph attention mechanism makes the effectiveness

⁵Although the edge adding strategy is hyperparameter-free, the ϵ is still there to distinguish the original graph and the rewired graph.

of DGAT more convincing, as elaborated in Section 5.2.

5. Experiments

In this section, we evaluate the effectiveness of our proposed DGAT on synthetic and real-world benchmark datasets. In Section 5.1, we conduct ablation experiments to validate the effectiveness of each proposed component in DGAT. In Section 5.2, we generate synthetic graphs with various homophily levels and shows that DGAT can outperform the baseline models in each homophily level. In Section 5.3, we compare DGAT with several baseline and state-of-the-art (SOTA) models on 7 real-world benchmark datasets and the results show that DGAT outperform the SOTA models on 6 out of 7 node classification tasks.

5.1. Ablation Study

This section conducts ablation studies to investigate the effectiveness of the usage of (1) parameterized normalized Laplacian $\mathbf{L}^{(\alpha, \gamma)}$, (2) the topology-guided graph rewiring strategy ($\mathcal{R}(\mathcal{G})$) and (3) the global directional attention (ATT_e) in DGAT. The results on 7 heterophily datasets are summarized in Table 1⁶.

It is observed from Table 1 that: (1) even without leveraging $\mathbf{L}^{(\alpha, \gamma)}$, *i.e.*, we only use the default \mathbf{L}_{rw} with $\alpha = 1, \gamma = 1$, the topology-guided graph rewiring strategy and the global directional attention can bring improvement individually; (2) after incorporating with $\mathbf{L}^{(\alpha, \gamma)}$ ⁷, the effectiveness of the above two components are further enhanced; (3) each component is indispensable for the success of DGAT and the full model performs the best on 6 out of 7 datasets (except for *amazon-ratings*⁸) when we combine the 3 components together.

⁶See Appendix F for the ablation study on the other 9 small-scale datasets (Pei et al., 2020).

⁷When $\mathbf{L}^{(\alpha, \gamma)}$ is utilized, we optimize α, γ for each graph to find the most suitable relative position for nodes.

⁸It can be explained by the results in (Platonov et al., 2023), which show that the GNNs yield negligible improvement over the graph-free models on *amazon-ratings*.

Representation Learning on Heterophilic Graph with Directional Neighborhood Attention

$L^{(\alpha, \gamma)}$	ATT _e	$\mathcal{R}(\mathcal{G})$	roman-empire	amazon-ratings	minesweeper	tolokers	questions	squirrel filtered	chameleon filtered
			80.87 ± 0.30	49.09 ± 0.63	92.01 ± 0.68	83.70 ± 0.47	77.43 ± 1.20	35.62 ± 2.06	39.21 ± 3.08
		✓	81.21 ± 0.71	47.27 ± 0.52	92.86 ± 0.53	84.28 ± 0.68	78.79 ± 1.01	40.45 ± 1.36	43.51 ± 5.06
	✓		82.50 ± 0.60	49.29 ± 0.57	92.07 ± 0.69	84.11 ± 0.41	OOM	36.50 ± 1.37	41.84 ± 2.76
✓		✓	82.27 ± 0.60	47.69 ± 0.64	92.94 ± 0.55	84.59 ± 0.53	78.97 ± 1.04	41.49 ± 2.72	43.89 ± 4.67
	✓	✓	86.82 ± 0.60	47.81 ± 0.54	93.15 ± 0.80	84.39 ± 0.49	OOM	41.48 ± 2.34	43.09 ± 4.13
✓	✓		83.01 ± 0.52	49.69 ± 0.51	92.15 ± 0.71	84.11 ± 0.41	78.66 ± 0.97	37.83 ± 1.54	43.37 ± 3.01
✓	✓	✓	87.27 ± 0.64	48.03 ± 0.58	93.27 ± 0.56	84.74 ± 0.59	79.55 ± 0.81	42.09 ± 2.65	44.16 ± 4.20

Table 1. Ablation study on heterophily datasets proposed by (Platonov et al., 2023). The checkmark on $L^{(\alpha, \gamma)}$ stands for adopting parameterized normalized Laplacian with optimal α and γ , while unchecking $L^{(\alpha, \gamma)}$ indicates that the default $L^{(1, 1)} = L_{rw}$ is used. The ATT_e stands for the global directional attention mechanism. And $\mathcal{R}(\mathcal{G})$ stands for graph re-wiring strategy. The OOM occurs for some specific choice of α and γ in computing eigenvectors. The best results are highlighted in **bold** format.

μ	GAT	GATv2	DGAT (γ^*)	DGAT (γ^-)
0.0	45.21	48.66	54.94 (0.1)	47.51 (0.7)
0.1	44.63	50.65	54.13 (0.3)	49.72 (0.9)
0.2	47.32	54.46	57.83 (0.3)	53.11 (1.0)
0.3	56.59	59.04	64.33 (0.3)	59.37 (1.0)
0.4	63.21	66.49	73.54 (0.3)	66.71 (0.7)
0.5	74.14	75.71	82.95 (0.7)	78.81 (0.2)
0.6	83.96	82.29	90.56 (0.7)	88.30 (0.5)
0.7	89.33	88.33	96.00 (0.9)	94.85 (0.4)
0.8	94.92	94.84	98.67 (0.6)	97.84 (0.5)
0.9	98.62	97.55	99.58 (0.8)	98.21 (0.1)

Table 2. Experimental results on synthetic graphs: average test accuracy (%) with different homophily coefficients. The results are averaged over 5 random splits. The best results are in **bold** format. For the DGAT model, we list the best and worst test runs (in the column DGAT (γ^*) and DGAT (γ^-) respectively) with different choices of γ in the bracket, e.g. 54.94(0.1) means that for $\gamma = 0.1$, the average test accuracy is 54.96%.

5.2. Synthetic Experiments

We follow (Karimi et al., 2018; Abu-El-Haija et al., 2019) to generate synthetic graphs characterized by a homophily coefficient $\mu \in \{0.0, 0.1, \dots, 0.9\}$, representing the chance that a node forms a connection to another node with the same label. We say the graph is more heterophilic for a smaller μ . A detailed explanation about how the synthetic graph are generated is given in Appendix C.2. We generate 5 synthetic graphs under each homophily coefficient μ . Node features are sampled from overlapping multi-Gaussian distributions. And for each generated graph, nodes are randomly partitioned into train/validation/test sets with a ratio of 60%/20%/20%. Each model is trained under the same hyperparameters setting with the learning rate of 0.01, the weight decay of 0.001 and the dropout rate of 0.1. The number of layers is set to be 2 for each model. And the attention-based model all use 8 heads with 8 hidden states per head.

In Table 2, the performance of DGAT are shown along with the fine-tuned hyperparameter γ in the bracket, while both the results under the optimal γ^* and the worst γ^- are presented. The DGAT(γ^*) outperforms remarkably better than the original GAT and GATv2 across all heterophily levels. Even with the worst γ^- , DGAT(γ^-) still achieve comparable or better results than baselines.

We can see that, as the graph becomes more heterophilic with a smaller μ , the optimal γ^* also decreases. Interestingly, γ^- has demonstrated a reverse correlation with μ . It aligned with Theorem 3.4 that if the graph has stronger heterophilic property, a large diffusion reduction with a smaller γ is preferred.

This observation provides a general guidance in searching for γ^* . See more detailed discussion about γ in Appendix C.3.

5.3. Experiments on Real-world Datasets

In this subsection, we compare DGAT with 6 baseline models: GAT (Velickovic et al., 2017), GAT-sep⁹, GCN (Kipf & Welling, 2016), SAGE (Hamilton et al., 2017), Graph Transformer (GT) (Shi et al., 2021) and GT-sep and 8 heterophily-specific SOTA models: H₂GCN (Zhu et al., 2020), CPGNN (Zhu et al., 2021), GPR-GNN (Chien et al., 2020), FSGNN (Maurya et al., 2022), GloGNN (Li et al., 2022), FAGCN (Bo et al., 2021), GBK-GNN (Du et al., 2022) and JacobiCov (Wang & Zhang, 2022) on 7 heterophily recently proposed benchmark datasets (Platonov et al., 2023): *roman-empire*, *amazon-ratings*, *minesweeper*, *tolokers*, *questions*, *Chameleon-filtered* and *Squirrel-filtered*.¹⁰

⁹“-sep” means to concatenate the ego feature of node and the aggregated neighborhood information, which is the trick used in (Platonov et al., 2023). We follow this setting.

¹⁰The overall statistics of these real-word datasets are given in Appendix C.1. We put the comparison results on the datasets from (Pei et al., 2020) in Appendix E. The reasons that we did show them in the main paper is that, those datasets are proved to have serious drawbacks, including duplicated nodes, small graph size and extreme class imbalance (Platonov et al., 2023). Thus, the

Representation Learning on Heterophilic Graph with Directional Neighborhood Attention

	roman-empire	amazon-ratings	minesweeper	tolokers	questions	squirrel-filtered	chameleon-filtered
GCN	73.69 ± 0.74	48.70 ± 0.63	89.75 ± 0.52	83.64 ± 0.67	76.09 ± 1.27	39.47 ± 1.47	40.89 ± 4.12
SAGE	85.74 ± 0.67	53.63 ± 0.39	93.51 ± 0.57	82.43 ± 0.44	76.44 ± 0.62	36.09 ± 1.99	37.77 ± 4.14
GAT	80.87 ± 0.30	49.09 ± 0.63	92.01 ± 0.68	83.70 ± 0.47	77.43 ± 1.20	35.62 ± 2.06	39.21 ± 3.08
GAT-sep	88.75 ± 0.41	52.70 ± 0.62	93.91 ± 0.35	83.78 ± 0.43	76.79 ± 0.71	35.46 ± 3.10	39.26 ± 2.50
GT	86.51 ± 0.73	51.17 ± 0.66	91.85 ± 0.76	83.23 ± 0.64	77.95 ± 0.68	36.30 ± 1.98	38.87 ± 3.66
GT-sep	87.32 ± 0.39	52.18 ± 0.80	92.29 ± 0.47	82.52 ± 0.92	78.05 ± 0.93	36.66 ± 1.63	40.31 ± 3.01
H ₂ GCN	60.11 ± 0.52	36.47 ± 0.23	89.71 ± 0.31	73.35 ± 1.01	63.59 ± 1.46	35.10 ± 1.15	26.75 ± 3.64
CPGNN	63.96 ± 0.62	39.79 ± 0.77	52.03 ± 5.46	73.36 ± 1.01	65.96 ± 1.95	30.04 ± 2.03	33.00 ± 3.15
GPR-GNN	64.85 ± 0.27	44.88 ± 0.34	86.24 ± 0.61	72.94 ± 0.97	55.48 ± 0.91	38.95 ± 1.99	39.93 ± 3.30
FSGNN	79.92 ± 0.56	52.74 ± 0.83	90.08 ± 0.70	82.76 ± 0.61	78.86 ± 0.92	35.92 ± 1.32	40.61 ± 2.97
GloGNN	59.63 ± 0.69	36.89 ± 0.14	51.08 ± 1.23	73.39 ± 1.17	65.74 ± 1.19	35.11 ± 1.24	25.90 ± 3.58
FAGCN	65.22 ± 0.56	44.12 ± 0.30	88.17 ± 0.73	77.75 ± 1.05	77.24 ± 1.26	41.08 ± 2.27	41.90 ± 2.72
GBK-GNN	74.57 ± 0.47	45.98 ± 0.71	90.85 ± 0.58	81.01 ± 0.67	74.47 ± 0.86	35.51 ± 1.65	39.61 ± 2.60
JacobiCov	71.14 ± 0.42	43.55 ± 0.48	89.66 ± 0.40	68.66 ± 0.65	73.88 ± 1.16	29.71 ± 1.66	39.00 ± 4.20
DGAT	87.27 ± 0.64	48.03 ± 0.58	93.27 ± 0.56	84.74 ± 0.59	79.55 ± 0.81	42.09 ± 2.65	44.16 ± 4.20
DGAT-sep	89.23 ± 0.56	50.60 ± 0.88	94.03 ± 0.45	84.83 ± 0.40	78.88 ± 0.94	39.69 ± 2.28	41.15 ± 4.66

Table 3. Experiment results on heterophily datasets proposed by (Platonov et al., 2023). Values stand for mean and standard deviation of evaluation metrics on the test datasets. Here *roman-empire*, *amazon-ratings*, *squirrel-filtered* and *chameleon-filtered* use accuracy for evaluation, while *minesweeper*, *tolokers* and *questions* use ROC AUC. The “sep” refers to the trick proposed in (Zhu et al., 2020) which concatenates node’s and the mean of neighbours’ embedding in each aggregation step, instead of adding them together. For fair comparison, we use the same experimental setup in (Platonov et al., 2023) for DGAT and DGAT-sep. Results for other models are reported by (Platonov et al., 2023). The top three results are highlighted in red, blue, and violet, respectively.

For the seven new heterophily datasets, we evaluate DGAT under the same experiment setting and fixed splits used (Platonov et al., 2023) with learning rate of $3 \cdot 10^{-5}$, weight decay of 0, dropout rate of 0.2, hidden dimension of 512 and attention head of 8, and number of layers from 1 to 5. Following (Platonov et al., 2023), DGAT is also trained for 1000 steps with Adam optimizer and select the best step based on the performance on the validation set.

The results are presented in Table 3, where GNNs baselines are organized in the beginning block, heterophily-specific GNNs are put in the second block.

Basically, DGAT achieve performance improvement compared with its base-model GAT (and DGAT-sep outperforms GAT-sep). And DGAT consistently surpasses SOTA GNNs that are specifically designed to deal with heterophily problems. While incorporating the “sep”-trick further enhances DGAT’s performance on *roman-empire*, *minesweeper* and *tolokers*. Since the “sep”-trick allows the aggregation step to put negative weights on the propagated message, which enables node-wise diversification that is proved to be useful on heterophily data (Luan et al., 2022a). In addition, the outstanding of DGAT from GT-based methods indicates that finding the useful graph for message propagation with sparse attention is more effective than considering the message passing between all pairs of nodes.

reliability of the comparison results is questionable.

6. Conclusion

In this work, we propose a novel parameterized normalized Laplacians, encompassing both the normalized Laplacian and the combinatorial Laplacian. With our proposed Laplacian, we design a Directional Graph Attention Network (DGAT) with controllable global directional flow that substantially enhances the expressiveness of the original Graph Attention Network (GAT) on a general graph. The two mechanisms proposed in this study have contributed to the improvement: the topology-guided neighbour rewiring and the global directional attention mechanism. The future research based on our work will focus on developing a quantitative guidance for selecting the parameter γ in the proposed parameterized normalized Laplacians.

References

- Abu-El-Haija, S., Perozzi, B., Kapoor, A., Alipourfard, N., Lerman, K., Harutyunyan, H., Ver Steeg, G., and Galstyan, A. Mixhop: Higher-order graph convolutional architectures via sparsified neighborhood mixing. In *International Conference on Machine Learning*, pp. 21–29. PMLR, 2019.
- Alon, U. and Yahav, E. On the bottleneck of graph neural networks and its practical implications. *arXiv preprint arXiv:2006.05205*, 2020.
- Arnaiz-Rodríguez, A., Begga, A., Escolano, F., and Oliver, N. Diffwire: Inductive graph rewiring via the Lovász bound. *arXiv preprint arXiv:2206.07369*, 2022.
- Beaini, D., Passaro, S., L’etourneau, V., Hamilton, W., Corso, G., and Li’o, P. Directional graph networks. In *Proceedings of the International Conference on Machine Learning*, pp. 748–758. PMLR, 2021.
- Belkin, M. and Niyogi, P. Laplacian eigenmaps for dimensionality reduction and data representation. *Neural Computation*, 15(6):1373–1396, 2003.
- Bo, D., Wang, X., Shi, C., and Shen, H. Beyond low-frequency information in graph convolutional networks. In *Proceedings of the AAAI Conference on Artificial Intelligence*, volume 35, pp. 3950–3957, 2021.
- Brody, S., Alon, U., and Yahav, E. How attentive are graph attention networks? *arXiv preprint arXiv:2105.14491*, 2021.
- Chien, E., Peng, J., Li, P., and Milenkovic, O. Adaptive universal generalized pagerank graph neural network. *arXiv preprint arXiv:2006.07988*, 2020.
- Coifman, R. R. and Lafon, S. Diffusion maps. *Applied and Computational Harmonic Analysis*, 21(1):5–30, 2006.
- Coifman, R. R., Lafon, S., Lee, A. B., Maggioni, M., Nadler, B., Warner, F., and Zucker, S. W. Geometric diffusions as a tool for harmonic analysis and structure definition of data: Diffusion maps. *Proceedings of the national academy of sciences*, 102(21):7426–7431, 2005.
- Du, L., Shi, X., Fu, Q., Ma, X., Liu, H., Han, S., and Zhang, D. Gbk-gnn: Gated bi-kernel graph neural networks for modeling both homophily and heterophily. In *Proceedings of the ACM Web Conference 2022*, pp. 1550–1558, 2022.
- Dwivedi, V. P. and Bresson, X. A generalization of transformer networks to graphs. *arXiv preprint arXiv:2012.09699*, 2020.
- Eliasof, M., Ruthotto, L., and Treister, E. Improving graph neural networks with learnable propagation operators. In *International Conference on Machine Learning*, pp. 9224–9245. PMLR, 2023.
- Hamilton, W. L. Graph representation learning. *Synthesis Lectures on Artificial Intelligence and Machine Learning*, 14(3):1–159, 2020.
- Hamilton, W. L., Ying, R., and Leskovec, J. Inductive representation learning on large graphs. In *Proceedings of the 31st International Conference on Neural Information Processing Systems*, pp. 1025–1035, 2017.
- He, M., Wei, Z., Xu, H., et al. Bernnet: Learning arbitrary graph spectral filters via bernstein approximation. *Advances in Neural Information Processing Systems*, 34, 2021.
- Hu, Z., Dong, Y., Wang, K., and Sun, Y. Heterogeneous graph transformer. In *Proceedings of the web conference 2020*, pp. 2704–2710, 2020.
- Hua, C., Luan, S., Xu, M., Ying, R., Fu, J., Ermon, S., and Precup, D. Mudiff: Unified diffusion for complete molecule generation. In *The Second Learning on Graphs Conference*, 2023.
- Karimi, F., Génois, M., Wagner, C., Singer, P., and Strohmaier, M. Homophily influences ranking of minorities in social networks. *Scientific Reports*, 8(1), jul 2018. doi: 10.1038/s41598-018-29405-7.
- Kim, Y. and Upfal, E. Algebraic connectivity of graphs, with applications. Bachelor’s thesis, Brown University, 2016.
- Kipf, T. N. and Welling, M. Semi-supervised classification with graph convolutional networks. *arXiv preprint arXiv:1609.02907*, 2016.
- Kreuzer, D., Beaini, D., Hamilton, W., L’etourneau, V., and Tossou, P. Rethinking graph transformers with spectral attention. *Advances in Neural Information Processing Systems*, 34:21618–21629, 2021.
- LeCun, Y., Bottou, L., Bengio, Y., and Haffner, P. Gradient-based learning applied to document recognition. *Proceedings of the IEEE*, 86(11):2278–2324, 1998.
- Lee, J. B., Rossi, R. A., Kim, S., Ahmed, N. K., and Koh, E. Attention models in graphs: A survey. *ACM Transactions on Knowledge Discovery from Data (TKDD)*, 13(6):1–25, 2019.
- Li, X., Zhu, R., Cheng, Y., Shan, C., Luo, S., Li, D., and Qian, W. Finding global homophily in graph neural networks when meeting heterophily. In *International Conference on Machine Learning*, pp. 13242–13256. PMLR, 2022.

- Lim, D., Li, X., Hohne, F., and Lim, S.-N. New benchmarks for learning on non-homophilous graphs. *arXiv preprint arXiv:2104.01404*, 2021.
- Liu, M., Wang, Z., and Ji, S. Non-local graph neural networks. *arXiv preprint arXiv:2005.14612*, 2020.
- Luan, S., Zhao, M., Chang, X.-W., and Precup, D. Break the ceiling: Stronger multi-scale deep graph convolutional networks. *Advances in neural information processing systems*, 32, 2019.
- Luan, S., Hua, C., Lu, Q., Zhu, J., Zhao, M., Zhang, S., Chang, X.-W., and Precup, D. Revisiting heterophily for graph neural networks. *Advances in neural information processing systems*, 35:1362–1375, 2022a.
- Luan, S., Zhao, M., Hua, C., Chang, X.-W., and Precup, D. Complete the missing half: Augmenting aggregation filtering with diversification for graph convolutional networks. In *NeurIPS 2022 Workshop: New Frontiers in Graph Learning*, 2022b.
- Luan, S., Hua, C., Lu, Q., Zhu, J., Chang, X.-W., and Precup, D. When do we need graph neural networks for node classification? *International Conference on Complex Networks and Their Applications*, 2023a.
- Luan, S., Hua, C., Xu, M., Lu, Q., Zhu, J., Chang, X.-W., Fu, J., Leskovec, J., and Precup, D. When do graph neural networks help with node classification? investigating the impact of homophily principle on node distinguishability. *Advances in Neural Information Processing Systems*, 36, 2023b.
- Maurya, S. K., Liu, X., and Murata, T. Simplifying approach to node classification in graph neural networks. *Journal of Computational Science*, 62:101695, 2022.
- McPherson, M., Smith-Lovin, L., and Cook, J. M. Birds of a feather: Homophily in social networks. *Annual Review of Sociology*, pp. 415–444, 2001.
- Muller, L., Galkin, M., Morris, C., and Rampasek, L. Attending to graph transformers. *arXiv preprint arXiv:2302.04181*, 2023.
- Nadler, B., Lafon, S., Kevrekidis, I., and Coifman, R. Diffusion maps, spectral clustering and eigenfunctions of fokker-planck operators. *Advances in neural information processing systems*, 18, 2005.
- Papp, P. A., Martinkus, K., Faber, L., and Wattenhofer, R. Dropgnn: Random dropouts increase the expressiveness of graph neural networks. *Advances in Neural Information Processing Systems*, 34:21997–22009, 2021.
- Pei, H., Wei, B., Chang, K. C.-C., Lei, Y., and Yang, B. Geom-gcn: Geometric graph convolutional networks. *arXiv preprint arXiv:2002.05287*, 2020.
- Platonov, O., Kuznedelev, D., Diskin, M., Babenko, A., and Prokhorenkova, L. A critical look at the evaluation of gnns under heterophily: are we really making progress? *arXiv preprint arXiv:2302.11640*, 2023.
- Qiu, H. and Hancock, E. R. Clustering and embedding using commute times. *IEEE Transactions on Pattern Analysis and Machine Intelligence*, 29(11):1873–1890, 2007.
- Rong, Y., Huang, W., Xu, T., and Huang, J. Dropedge: Towards deep graph convolutional networks on node classification. *arXiv Preprint arXiv:1907.10903*, 2019.
- Scarselli, F., Gori, M., Tsoi, A. C., Hagenbuchner, M., and Monfardini, G. The graph neural network model. *IEEE Transactions on Neural Networks*, 20(1):61–80, 2008.
- Shi, Y., Huang, Z., Feng, S., Zhong, H., Wang, W., and Sun, Y. Masked label prediction: Unified message passing model for semi-supervised classification, 2021.
- Topping, J., Di Giovanni, F., Chamberlain, B. P., Dong, X., and Bronstein, M. M. Understanding over-squashing and bottlenecks on graphs via curvature. *arXiv preprint arXiv:2111.14522*, 2021.
- Vaswani, A., Shazeer, N., Parmar, N., Uszkoreit, J., Jones, L., Gomez, A. N., Kaiser, L., and Polosukhin, I. Attention is all you need. *Advances in Neural Information Processing Systems*, 30, 2017.
- Velickovic, P., Cucurull, G., Casanova, A., Romero, A., Lio, P., and Bengio, Y. Graph attention networks. *arXiv preprint arXiv:1710.10903*, 2017.
- Wang, G., Ying, R., Huang, J., and Leskovec, J. Direct multi-hop attention based graph neural network. *arXiv preprint arXiv:2009.14332*, 2020.
- Wang, X. and Zhang, M. How powerful are spectral graph neural networks. In *International Conference on Machine Learning*, pp. 23341–23362. PMLR, 2022.
- Xu, K., Hu, W., Leskovec, J., and Jegelka, S. How powerful are graph neural networks? *arXiv preprint arXiv:1810.00826*, 2018.
- Yun, S., Jeong, M., Kim, R., Kang, J., and Kim, H. J. Graph transformer networks. *Advances in neural information processing systems*, 32, 2019.
- Zhao, M., Liu, Z., Luan, S., Zhang, S., Precup, D., and Bengio, Y. A consciousness-inspired planning agent for model-based reinforcement learning. *Advances in neural information processing systems*, 34:1569–1581, 2021.

- Zheng, X., Liu, Y., Pan, S., Zhang, M., Jin, D., and Yu, P. S. Graph neural networks for graphs with heterophily: A survey. *arXiv preprint arXiv:2202.07082*, 2022.
- Zhu, J., Yan, Y., Zhao, L., Heimann, M., Akoglu, L., and Koutra, D. Beyond homophily in graph neural networks: Current limitations and effective designs. *Advances in Neural Information Processing Systems*, 33:7793–7804, 2020.
- Zhu, J., Rossi, R. A., Rao, A., Mai, T., Lipka, N., Ahmed, N. K., and Koutra, D. Graph neural networks with heterophily. In *Proceedings of the AAAI conference on artificial intelligence*, volume 35, pp. 11168–11176, 2021.

A. Homophily Metrics

In addition to the node homophily metric introduced in (11), here we review some commonly used metrics to measure homophily. We denote $\mathbf{z} \in \mathbb{R}^N$ as labels of nodes, and $\mathbf{Z} \in \mathbb{R}^{N \times C}$ as the one-hot encoding of labels, where C is the number of classes. Edge homophily H_{edge} is defined as follows:

$$H_{\text{edge}} = \frac{|\{e_{ij} | e_{ij} \in \mathcal{E}, \mathbf{z}_i = \mathbf{z}_j\}|}{|\mathcal{E}|}. \quad (23)$$

Adjusted edge homophily H_{edge}^* considers classes imbalance and is defined as (Platonov et al., 2023):

$$H_{\text{edge}}^* = \frac{H_{\text{edge}} - \sum_c p^2(c)}{1 - \sum_c p^2(c)}. \quad (24)$$

Here $p(c) = \sum_{i:\mathbf{z}_i=c} \mathbf{D}_{ii} / (2|\mathcal{E}|)$, $c = 1 : C$, defines the degree-weighted distribution of class labels. The class homophily is also proposed to take class imbalance into account (Lim et al., 2021):

$$H_{\text{class}} = \frac{1}{C-1} \sum_c \left[h_c - \frac{|\{v_i | \mathbf{z}_i = c\}|}{N} \right]_+ \quad (25)$$

$$h_c = \frac{\sum_{v_i:\mathbf{z}_i=c} |\{e_{ij} | e_{ij} \in \mathcal{E}, \mathbf{z}_i = \mathbf{z}_j\}|}{\sum_{v_i:\mathbf{z}_i=c} \mathbf{D}_{ii}}. \quad (26)$$

Label informativeness, which indicates the amount of information a neighbor’s label provides about node’s label, is defined as follows (Platonov et al., 2023):

$$LI = 2 - \frac{\sum_{c_1, c_2} p(c_1, c_2) \log p(c_1, c_2)}{\sum_c p(c) \log p(c)}, \quad (27)$$

where $p(c_1, c_2) = |\{e_{ij} | e_{ij} \in \mathcal{E}, \mathbf{z}_i = c_1, \mathbf{z}_j = c_2\}| / (2|\mathcal{E}|)$. The aggregation homophily $H_{\text{agg}}^M(\mathcal{G})$ measures the proportion of nodes that assign greater average weights to intra-class nodes than inter-class nodes. It is defined as follows (Luan et al., 2022a):

$$H_{\text{agg}}^M(\mathcal{G}) = \frac{1}{|\mathcal{V}|} \left| \{v_i | \text{Mean}_j(\{S(\hat{\mathbf{A}}, \mathbf{Z})_{ij} | \mathbf{z}_i = \mathbf{z}_j\}) \geq \text{Mean}_j(\{S(\hat{\mathbf{A}}, \mathbf{Z})_{ij} | \mathbf{z}_i \neq \mathbf{z}_j\}) \} \right|, \quad (28)$$

where $S(\hat{\mathbf{A}}, \mathbf{Z}) = \hat{\mathbf{A}}\mathbf{Z}(\hat{\mathbf{A}}\mathbf{Z})^T$ defines the post-aggregation node similarity, with $\hat{\mathbf{A}} = \mathbf{A} + \mathbf{I}$, and $\text{Mean}_j(\{\cdot\})$ takes the average over node v_j of a given multiset of values. Under the homophily metrics mentioned above, a smaller value indicates a higher degree of heterophily. While H_{edge}^* can assume negative values, the other metrics fall within the range $[0, 1]$.

B. Proof of Theorem

B.1. Proof of theorem 3.2

Proof. By Definition 3.1, we have

$$\begin{aligned} \mathbf{P}^{(\alpha, \gamma)} &= \mathbf{I} - \mathbf{L}^{(\alpha, \gamma)} = \mathbf{I} - \gamma[\gamma\mathbf{D} + (1-\gamma)\mathbf{I}]^{-\alpha} \mathbf{L}[\gamma\mathbf{D} + (1-\gamma)\mathbf{I}]^{\alpha-1} \\ &= [\gamma\mathbf{D} + (1-\gamma)\mathbf{I}]^{-\alpha} [\gamma\mathbf{D} + (1-\gamma)\mathbf{I} - \gamma\mathbf{L}] [\gamma\mathbf{D} + (1-\gamma)\mathbf{I}]^{\alpha-1} \\ &= [\gamma\mathbf{D} + (1-\gamma)\mathbf{I}]^{-\alpha} [\gamma\mathbf{A} + (1-\gamma)\mathbf{I}] [\gamma\mathbf{D} + (1-\gamma)\mathbf{I}]^{\alpha-1}. \end{aligned}$$

It is easy to see that all elements in $\mathbf{P}^{(\alpha, \gamma)}$ are non-negative. Since $\mathbf{A}\mathbf{1} = \mathbf{D}\mathbf{1}$, we have

$$\mathbf{P}^{(1, \gamma)} \mathbf{1} = (\gamma\mathbf{D} + (1-\gamma)\mathbf{I})^{-1} (\gamma\mathbf{A} + (1-\gamma)\mathbf{I}) \mathbf{1} = \mathbf{1},$$

completing the proof. \square

B.2. Proof of theorem 3.3

Proof. For any nonzero $\mathbf{x} \in \mathbb{R}^N$, write $\mathbf{y} := [\gamma\mathbf{D} + (1-\gamma)\mathbf{I}]^{-1/2} \mathbf{x}$. Then we have

$$\begin{aligned} \frac{\mathbf{x}^T \mathbf{L}^{(1/2, \gamma)} \mathbf{x}}{\mathbf{x}^T \mathbf{x}} &= \frac{\mathbf{x}^T \gamma [\gamma\mathbf{D} + (1-\gamma)\mathbf{I}]^{-1/2} \mathbf{L} [\gamma\mathbf{D} + (1-\gamma)\mathbf{I}]^{-1/2} \mathbf{x}}{\mathbf{x}^T \mathbf{x}} \\ &= \frac{\gamma \mathbf{y}^T \mathbf{L} \mathbf{y}}{\mathbf{y}^T [\gamma\mathbf{D} + (1-\gamma)\mathbf{I}] \mathbf{y}} = \frac{\frac{\gamma}{2} \sum_{ij} a_{ij} (y_i - y_j)^2}{\gamma \sum_{ij} a_{ij} y_i^2 + (1-\gamma) \sum_i y_i^2}. \end{aligned}$$

By the Rayleigh quotient theorem,

$$\lambda^{(0)}(\gamma) = \min_{\mathbf{y} \neq \mathbf{0}} \frac{\frac{\gamma}{2} \sum_{ij} a_{ij} (y_i - y_j)^2}{\gamma \sum_{ij} a_{ij} y_i^2 + (1-\gamma) \sum_i y_i^2} = 0, \quad (29)$$

where the minimum is reached when \mathbf{y} is a multiple of $\mathbf{1}$ and

$$\begin{aligned} \lambda^{(N-1)}(\gamma) &= \max_{\mathbf{y} \neq \mathbf{0}} \frac{\frac{\gamma}{2} \sum_{ij} a_{ij} (y_i - y_j)^2}{\gamma \sum_{ij} a_{ij} y_i^2 + (1-\gamma) \sum_i y_i^2} \\ &\leq \max_{\mathbf{y} \neq \mathbf{0}} \frac{\sum_{ij} a_{ij} (y_i^2 + y_j^2)}{\sum_{ij} a_{ij} y_i^2} \leq 2, \end{aligned}$$

leading to Eq. (15). The proof of showing $\lambda^{(1)}(\gamma) \neq 0$ if and only if \mathcal{G} is connected is similar to (Kim & Upfal, 2016), thus we omit the details here.

By the Courant-Fischer min-max theorem, for $\gamma \neq 0$,

$$\begin{aligned} \lambda^{(i)}(\gamma) &= \min_{\{S: \dim(S)=i+1\}} \max_{\{\mathbf{x}: \mathbf{0} \neq \mathbf{x} \in S\}} \frac{\mathbf{x}^T \mathbf{L}^{(1/2, \gamma)} \mathbf{x}}{\mathbf{x}^T \mathbf{x}} \\ &= \min_{\{S: \dim(S)=i+1\}} \max_{\{\mathbf{y}: \mathbf{0} \neq \mathbf{y} \in S\}} \frac{\mathbf{y}^T \mathbf{L} \mathbf{y}}{\mathbf{y}^T [\mathbf{D} - \mathbf{I} + (1/\gamma)\mathbf{I}] \mathbf{y}}. \end{aligned}$$

It is obvious that the Rayleigh quotient $\frac{\mathbf{y}^T \mathbf{L} \mathbf{y}}{\mathbf{y}^T [\mathbf{D} - \mathbf{I} + (1/\gamma)\mathbf{I}] \mathbf{y}}$ is strictly increasing with respect to $\gamma \in (0, 1]$ if $\mathbf{L} \mathbf{y} \neq \mathbf{0}$, i.e., \mathbf{y} not a multiple of $\mathbf{1}$. Note that $\lambda^{(0)}(\gamma) = 0$ and it is reached when $\mathbf{L} \mathbf{y} = \mathbf{0}$, or equivalently \mathbf{y} is a multiple of $\mathbf{1}$. Thus, $\lambda^{(i)}(\gamma)$ is strictly increasing with respect to γ for $i = 1 : N - 1$.

From the eigendecomposition of the symmetric $\mathbf{L}^{(1/2,\gamma)}$ in (14), we can find the eigendecomposition of $\mathbf{L}^{(\alpha,\gamma)}$ as follows:

$$\begin{aligned} \mathbf{L}^{(\alpha,\gamma)} &= [\gamma \mathbf{D} + (1-\gamma)\mathbf{I}]^{1/2-\alpha} \mathbf{L}^{(1/2,\gamma)} [\gamma \mathbf{D} + (1-\gamma)\mathbf{I}]^{\alpha-1/2} \\ &= [\gamma \mathbf{D} + (1-\gamma)\mathbf{I}]^{1/2-\alpha} (\mathbf{U} \mathbf{\Lambda}^{(\gamma)} \mathbf{U}^T) [\gamma \mathbf{D} + (1-\gamma)\mathbf{I}]^{\alpha-1/2} \\ &= ([\gamma \mathbf{D} + (1-\gamma)\mathbf{I}]^{1/2-\alpha} \mathbf{U}) \mathbf{\Lambda}^{(\gamma)} ([\gamma \mathbf{D} + (1-\gamma)\mathbf{I}]^{1/2-\alpha} \mathbf{U})^{-1} \end{aligned}$$

Thus, $\lambda^{(i)}(\gamma)$ is also an eigenvalue of $\mathbf{L}^{(\alpha,\gamma)}$ for $i = 0 : N-1$, and the i -th column of $[\gamma \mathbf{D} + (1-\gamma)\mathbf{I}]^{1/2-\alpha} \mathbf{U}$ is a corresponding eigenvector. \square

B.3. Proof of Theorem 3.4

Proof. The proof is similar to the proof of (Beaini et al., 2021). By (Coifman & Lafon, 2006), the diffusion distance at time t between node v_i and v_j can be expressed as:

$$d_t(v_i, v_j) = \left(\sum_{k=1}^{n-1} e^{-2t\lambda^{(k)}(\gamma)} (\phi_i^{(k)}(\gamma) - \phi_j^{(k)}(\gamma))^2 \right)^{\frac{1}{2}}, \quad (30)$$

where $\lambda^{(1)}(\gamma) \leq \lambda^{(2)}(\gamma) \leq \dots \leq \lambda^{(n-1)}(\gamma)$ are eigenvalues of $\mathbf{L}^{(1,\gamma)}$, and $\{\phi^{(1)}(\gamma), \phi^{(2)}(\gamma), \dots, \phi^{(n-1)}(\gamma)\}$ are the corresponding eigenvectors. We omit the zero $\lambda^{(0)}(\gamma)$. The inequality $d_t(v_m, v_j) < d_t(v_i, v_j)$ is then equivalent as

$$\begin{aligned} & \left(\sum_{k=1}^{n-1} e^{-2t\lambda^{(k)}(\gamma)} (\phi_m^{(k)}(\gamma) - \phi_j^{(k)}(\gamma))^2 \right)^{\frac{1}{2}} \\ & < \left(\sum_{k=1}^{n-1} e^{-2t\lambda^{(k)}(\gamma)} (\phi_i^{(k)}(\gamma) - \phi_j^{(k)}(\gamma))^2 \right)^{\frac{1}{2}}. \end{aligned} \quad (31)$$

We can take out $\lambda^{(1)}(\gamma)$ and $\phi^{(1)}(\gamma)$ and rearrange the above inequality as:

$$\begin{aligned} & \sum_{k=2}^{n-1} e^{-2t\lambda^{(k)}(\gamma)} \left((\phi_m^{(k)}(\gamma) - \phi_j^{(k)}(\gamma))^2 - (\phi_i^{(k)}(\gamma) - \phi_j^{(k)}(\gamma))^2 \right) \\ & < e^{-2t\lambda^{(1)}(\gamma)} \left((\phi_i^{(1)}(\gamma) - \phi_j^{(1)}(\gamma))^2 - (\phi_m^{(1)}(\gamma) - \phi_j^{(1)}(\gamma))^2 \right). \end{aligned} \quad (32)$$

The left-hand side of Eq. (32) has an upper bound:

$$\begin{aligned} & \sum_{k=2}^{n-1} e^{-2t\lambda^{(k)}(\gamma)} \left| (\phi_m^{(k)}(\gamma) - \phi_j^{(k)}(\gamma))^2 - (\phi_i^{(k)}(\gamma) - \phi_j^{(k)}(\gamma))^2 \right| \\ & \leq e^{-2t\lambda^{(2)}(\gamma)} \sum_{k=2}^{n-1} \left| (\phi_m^{(k)}(\gamma) - \phi_j^{(k)}(\gamma))^2 - (\phi_i^{(k)}(\gamma) - \phi_j^{(k)}(\gamma))^2 \right|. \end{aligned} \quad (33)$$

Then Eq. (32) holds if:

$$\begin{aligned} & e^{-2t\lambda^{(2)}(\gamma)} \sum_{k=2}^{n-1} \left| (\phi_m^{(k)}(\gamma) - \phi_j^{(k)}(\gamma))^2 - (\phi_i^{(k)}(\gamma) - \phi_j^{(k)}(\gamma))^2 \right| \\ & \leq e^{-2t\lambda^{(1)}(\gamma)} \left((\phi_i^{(1)}(\gamma) - \phi_j^{(1)}(\gamma))^2 - (\phi_m^{(1)}(\gamma) - \phi_j^{(1)}(\gamma))^2 \right), \end{aligned} \quad (34)$$

which is equivalent to

$$\begin{aligned} & \log \left(\frac{(\phi_i^{(1)}(\gamma) - \phi_j^{(1)}(\gamma))^2 - (\phi_m^{(1)}(\gamma) - \phi_j^{(1)}(\gamma))^2}{\sum_{k=2}^{n-1} \left| (\phi_m^{(k)}(\gamma) - \phi_j^{(k)}(\gamma))^2 - (\phi_i^{(k)}(\gamma) - \phi_j^{(k)}(\gamma))^2 \right|} \right) \\ & \times \frac{1}{2(\lambda^{(1)}(\gamma) - \lambda^{(2)}(\gamma))} < t. \end{aligned} \quad (35)$$

Let the constant C be the left-hand side of Eq. (35), then if we take $t \geq \lfloor C \rfloor + 1$, we have $d_t(v_m, v_j) < d_t(v_i, v_j)$. Note that C exists if

$$\frac{(\phi_i^{(1)}(\gamma) - \phi_j^{(1)}(\gamma))^2 - (\phi_m^{(1)}(\gamma) - \phi_j^{(1)}(\gamma))^2}{\sum_{k=2}^{n-1} \left| (\phi_m^{(k)}(\gamma) - \phi_j^{(k)}(\gamma))^2 - (\phi_i^{(k)}(\gamma) - \phi_j^{(k)}(\gamma))^2 \right|} > 0, \quad (36)$$

which is satisfied since we assume $|\phi_i^{(1)}(\gamma) - \phi_j^{(1)}(\gamma)| > |\phi_m^{(1)}(\gamma) - \phi_j^{(1)}(\gamma)|$. The original theorem (Beaini et al., 2021) is only based on $\phi^{(1)}$ and does not assume that v_m must satisfy $|\phi_i^{(1)} - \phi_j^{(1)}| > |\phi_m^{(1)} - \phi_j^{(1)}|$, which is necessary for the existence of C . In addition, the original theorem (Beaini et al., 2021) assumes that v_m is obtained by taking a gradient step from v_i , i.e., $\phi_m - \phi_i = \max_{j: v_j \in \mathcal{N}(v_i)} (\phi_j - \phi_i)$, while this property is not needed for the proof. Therefore, Theorem 3.4 both extends and overcomes the shortcomings of (Beaini et al., 2021). \square

C. Datasets

C.1. Real-world Datasets

The overall statistics of the real-world datasets are presented in Table C.1 and Table C.1 provides their heterophily levels calculated using various homophily metrics.

	#Nodes	#Edges	#Features	#Classes	Metric
chameleon	2,277	31,371	2,325	5	ACC
squirrel	5,201	198,353	2,089	5	ACC
actor	7,600	26,659	932	5	ACC
cornell	183	277	1,703	5	ACC
wisconsin	251	450	1,703	5	ACC
texas	183	279	1,703	5	ACC
cora	2,708	5,278	1,433	7	ACC
citeseer	3,327	4,552	3,703	6	ACC
pubmed	19,717	44,324	500	3	ACC
roman-empire	22,662	32,927	300	18	ACC
amazon-ratings	24,492	93,050	300	5	ACC
minesweeper	10,000	39,402	7	2	ROC AUC
tolokers	11,758	519,000	10	2	ROC AUC
questions	48,921	153,540	301	2	ROC AUC
squirrel-filtered	2,223	46,998	2,089	5	ACC
chameleon-filtered	890	8,854	2,325	5	ACC

Table 4. Statistics of the benchmark dataset. Following pre-processing, the graph has been transformed into an undirected and simple form, without self-loops or multiple edges.

	H_{node}	H_{edge}	H_{class}	$H_{\text{agg}}^{\text{M}}(\mathcal{G})$	H_{edge}^*	LI
chameleon	0.25	0.23	0.04	0.36	0.03	0.05
squirrel	0.22	0.22	0.03	0.00	0.01	0.00
actor	0.22	0.22	0.01	0.62	0.00	0.00
cornell	0.30	0.30	0.02	0.02	-0.08	0.02
wisconsin	0.16	0.18	0.05	0.00	-0.17	0.13
texas	0.06	0.06	0.00	0.00	-0.29	0.19
cora	0.83	0.81	0.77	0.99	0.77	0.59
citeseer	0.71	0.74	0.63	0.97	0.67	0.45
pubmed	0.79	0.80	0.66	0.94	0.69	0.41
roman-empire	0.05	0.05	0.02	1.00	-0.05	0.11
amazon-ratings	0.38	0.38	0.13	0.60	0.14	0.04
minesweeper	0.68	0.68	0.01	0.61	0.01	0.00
tolokers	0.63	0.59	0.18	0.00	0.09	0.01
questions	0.90	0.84	0.08	0.00	0.02	0.00
squirrel-filtered	0.19	0.21	0.04	0.00	0.01	0.00
chameleon-filtered	0.24	0.24	0.04	0.25	0.03	0.01

Table 5. Heterophily levels of benchmark datasets. The $H_{\text{agg}}^{\text{M}}(\mathcal{G})$ stands for the aggregation homophily, calculated using $\hat{\mathbf{A}} = \mathbf{A} + \mathbf{I}$. The H_{edge}^* stands for the adjusted edge homophily, and the LI stands for the label informativeness. The definitions of these metrics can be found in (11) and in Appendix A.

C.2. Synthetic Datasets

In addition to the real-world datasets, we also tested the DGAT model on synthetic graphs generated with different homophily levels ranging from 0 to 1 using the method proposed in (Abu-El-Haija et al., 2019). Here we give a review of the generation process.

More specifically, when generating the output graph \mathcal{G} with a desired total number of nodes N , a total of C classes, and a homophily coefficient μ , the process begins by dividing the N nodes into C equal-sized classes. Then the synthetic graph \mathcal{G} (initially empty) is updated iteratively. At each step, a new node v_i is added, and its class z_i is randomly assigned from the set $\{1, \dots, C\}$. Whenever a new node v_i is added to the graph, we establish a connection between it and an existing node v_j in \mathcal{G} based on the probability p_{ij} determined by the following rules:

$$p_{ij} = \begin{cases} d_j \times \mu, & \text{if } z_i = z_j \\ d_j \times (1 - \mu) \times w_{d(z_i, z_j)}, & \text{otherwise} \end{cases}. \quad (37)$$

where z_i and z_j are class labels of node i and j respectively, and $w_{d(z_i, z_j)}$ denotes the ‘‘cost’’ of connecting nodes from two distinct classes with a class distance of $d(z_i, z_j)$. For a larger μ , the chance of connecting with a node with the same label increases. The distance between two classes simply implies the shortest distance between the two classes on a circle where classes are numbered from 1 to C . For instance, if $C = 6$, $z_i = 1$ and $z_j = 5$, then the distance between z_i and z_j is 2. The weight exponentially decreases as the distance increases and is normalized such that $\sum_d w_d = 1$. In addition, the probability p_{ij} defined in Eq. (37) is also

normalized over the existing nodes:

$$\bar{p}_{ij} = \frac{p_{ij}}{\sum_{k: v_k \in \mathcal{N}(v_i)} p_{ik}}$$

Lastly, the features of each node in the output graph are sampled from overlapping 2D Gaussian distributions. Each class has its own distribution defined separately.

C.3. On the choice of γ for synthetic graphs

We use the performance of a 1-layer GCN on the synthetic graphs¹¹ to further illustrate how the hyper-parameter γ in $\mathbf{L}^{(1, \gamma)}$ influences the effectiveness of graph message passing under different heterophily levels. As defined in (13), the parameterized normalized adjacent matrix for $\mathbf{L}^{(1, \gamma)}$ is

$$\mathbf{P}^{(1, \gamma)} = (\gamma \mathbf{D} + (1 - \gamma) \mathbf{I})^{-1} (\gamma \mathbf{A} + (1 - \gamma) \mathbf{I}).$$

Then the output of a 1-layer GCN with aggregation weights defined by $\mathbf{P}^{(1, \gamma)}$ can be expressed as

$$\text{softmax}(\text{ReLU}(\mathbf{P}^{(1, \gamma)} \mathbf{X} \mathbf{W}_0) \mathbf{W}_1).$$

As the Figure 2 shows, generally, the performance of GCN increases with μ . The optimal γ increases as the graph becomes less homophilic, which aligns with results in Section 5.2 and Theorem 3.4. Furthermore, in the case of heterophily ($\mu < 0.5$), a larger γ tends to have a detrimental effect on performance. With the increase of μ , the influence on performance brought by a larger γ gradually changes from negative to positive.

D. Training

In training and evaluating a model using a node classification benchmark dataset with C distinct classes, each node $v_i \in \mathcal{V}$ has a label z_i associated with it. We denote $\mathbf{Z} \in \mathbb{R}^{N \times C}$ as the one-hot encoding of labels. Moreover, nodes are divided into three sets: the training set $\mathcal{V}_{\text{train}}$, the validation set \mathcal{V}_{val} and the test set $\mathcal{V}_{\text{test}}$. In the training phase, the model uses features of all nodes under transductive learning. The model only has access to labels of nodes in $\mathcal{V}_{\text{train}}$ and in \mathcal{V}_{val} (for hyperparameter tuning), while labels of nodes in $\mathcal{V}_{\text{test}} = \mathcal{V} \setminus (\mathcal{V}_{\text{train}} \cup \mathcal{V}_{\text{val}})$ remain unknown to the model.

The cost function used in node classification tasks is the standard categorical cross-entropy loss (Hamilton, 2020), which is commonly used for multi-class classification tasks:

$$\mathcal{L} = -\frac{1}{|\mathcal{V}_{\text{train}}|} \text{trace}(\mathbf{Z}^{\text{T}} \log \mathbf{Y}), \quad (38)$$

where \mathbf{Y} is the output from the model after softmax and $\log(\cdot)$ is applied element-wise.

¹¹The training use the same setting as Section 5.2, where the learning rate of 0.01, the weight decay of 0.001, the dropout rate of 0.1, and the hidden dimension of 64 are used.

$\mathcal{R}(\mathcal{G})$		✓	✓		✓	✓	✓
ATT_e				✓	✓	✓	✓
$\mathbf{L}^{(\alpha,\gamma)}$			✓		✓		✓
chameleon	42.93	51.71 ± 1.23	51.91 ± 1.59	46.69 ± 1.98	46.95 ± 2.50	52.39 ± 2.08	52.47 ± 1.44
squirrel	30.03	32.91 ± 2.26	34.70 ± 1.02	34.67 ± 0.10	34.71 ± 1.02	33.93 ± 1.86	34.82 ± 1.60
actor	28.45	35.24 ± 1.07	35.51 ± 0.74	29.63 ± 0.52	29.87 ± 0.60	35.64 ± 0.10	35.68 ± 1.20
cornell	54.32	82.16 ± 5.94	84.32 ± 4.15	60.27 ± 4.02	60.54 ± 0.40	84.86 ± 5.12	85.14 ± 5.30
wisconsin	49.41	83.92 ± 3.59	84.12 ± 3.09	54.51 ± 7.68	54.71 ± 5.68	84.11 ± 2.69	84.71 ± 3.59
texas	58.38	78.38 ± 5.13	78.65 ± 4.43	60.81 ± 5.16	60.81 ± 4.87	78.92 ± 5.57	79.46 ± 3.67
cora	86.37	87.85 ± 1.02	87.83 ± 1.20	87.95 ± 1.01	87.28 ± 1.53	87.93 ± 0.99	88.05 ± 1.09
citeseer	74.32	74.50 ± 1.99	76.18 ± 1.35	76.31 ± 1.38	76.41 ± 1.62	73.91 ± 1.62	76.41 ± 1.45
pubmed	87.62	87.78 ± 0.44	87.93 ± 0.36	87.90 ± 0.40	87.88 ± 0.46	87.82 ± 0.30	87.94 ± 0.48

Table 6. Ablation study on 9 real-world datasets (Pei et al., 2020). Cell with ✓ means the component is applied to the DGAT model. The $\mathbf{L}^{(\alpha,\gamma)}$ means that the parameterized normalized Laplacian is used with optimal α and γ , while unchecking $\mathbf{L}^{(\alpha,\gamma)}$ indicates that the default $\mathbf{L}^{(1,1)} = \mathbf{L}_{\text{rw}}$ is used. The ATT_e is the global directional attention mechanism. And $\mathcal{R}(\mathcal{G})$ is the graph re-wiring strategy. DGAT without all component is just GAT, whose results are reported from (Pei et al., 2020). The best test results are highlighted in bold format.

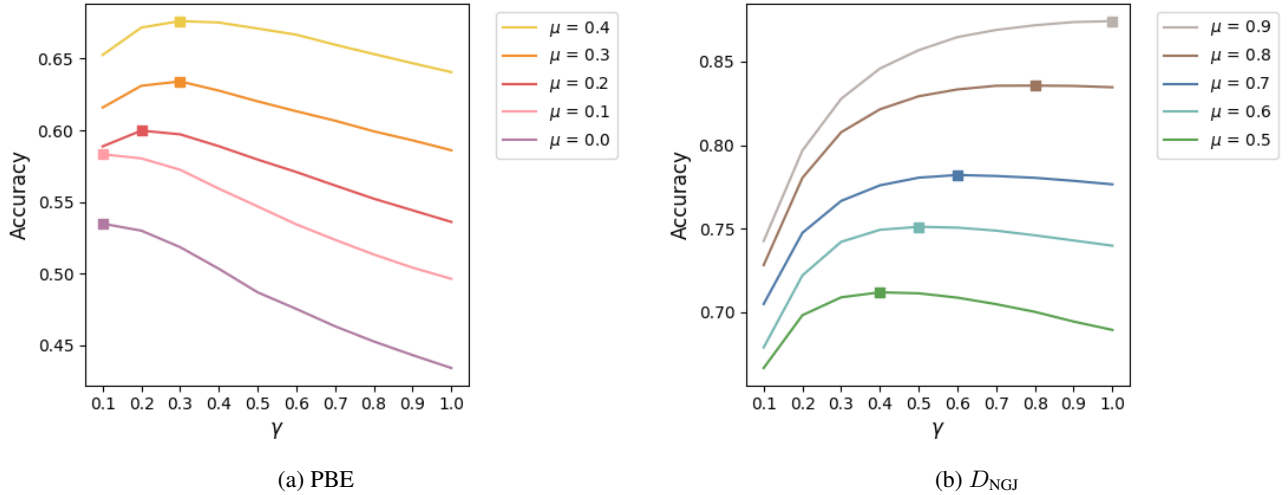


Figure 2. The performance of a one layer GCN with aggregation weights defined by $\mathbf{P}^{(1,\gamma)}$ on synthetic graphs. Results are shown separately for heterophily ($\mu < 0.5$) on the left panel and homophily ($\mu \geq 0.5$) on the right, with the solid line as the mean accuracy over 5 splits. The optimal γ for each μ is highlighted using square.

E. Additional Benchmark Results

The benchmark on the 9 small real-world datasets from (Pei et al., 2020), namely *chameleon*, *squirrel*, *actor*, *cornell*, *wisconsin*, *texas*, *cora*, *citeseer* and *pubmed*, demonstrates that DGAT combines the advantages of GAT and DGN. The experiments use 10 fixed splits from (Pei et al., 2020), which divide nodes into 48%/32%/20%. We perform a grid search for the hyperparameters of DGN according to (Beaini et al., 2021) for the learning rate in $\{10^{-5}, 10^{-4}\}$, the weight decay in $\{10^{-6}, 10^{-5}\}$, the dropout rate in $\{0.3, 0.5\}$, the aggregator in $\{\text{“mean-dir1-av”}, \text{“mean-dir1-dx”}, \text{“mean-dir1-av-dir1-dx”}\}$, the net type in $\{\text{“complex”}, \text{“simple”}\}$. DGAT adopts the same training setting as GAT, which consists of 2 layers, 8 heads and same hidden size for each datasets. The hidden size is set to 48 for *chameleon* and *squirrel*, 32 for *actor*, *cornell*, *wisconsin* and *texas*, 16 for *cora* and *citeseer*, and 64 for *pubmed*. All methods are trained using the Adam optimizer with 1000 steps. Table 7 gives the optimal hyperparameters for DGAT on 9 real-world dataset from (Pei et al., 2020).

Comparing DGAT against GAT and DGN, the results in Table 8 demonstrate that DGAT enhances both graph attention and directional aggregation by incorporating directional information into the computation of graph attention. We observed that DGAT outperforms GAT on all datasets, particularly those with pronounced heterophilic characteristics, namely, *chameleon*, *squirrel*, *actor*, *cornell*, *wisconsin* and *texas*. As shown in (Beaini et al., 2021), DGN holds advantages over GAT due to its inherent anisotropic nature. Table 8 provides further evidence to support this argument. In addition, the results show the superior improvement of DGAT compared to DGN across all homophilic datasets, namely, *cora*, *citeseer* and *pubmed*. This outcome serves as evidence that our proposed model effectively combines the advantages of both mechanisms.

Dataset ($H_{\text{node}}(\mathcal{G})$)	learning rate	weight decay	dropout	ϵ	γ	α
chameleon (0.25)	5×10^{-3}	5×10^{-4}	0.4	1×10^{-7}	0.0	0.9
squirrel (0.22)	5×10^{-2}	5×10^{-5}	0.2	1×10^{-7}	0.2	0.1
actor (0.22)	1×10^{-5}	1×10^{-7}	0.3	1×10^{-7}	0.2	0.2
cornell (0.30)	5×10^{-3}	5×10^{-4}	0.2	5×10^{-6}	0.3	0.8
wisconsin (0.16)	5×10^{-3}	5×10^{-6}	0.5	1×10^{-6}	0.3	0.7
texas (0.06)	5×10^{-5}	5×10^{-3}	0.4	1×10^{-5}	0.2	0.8
cora (0.83)	5×10^{-3}	5×10^{-4}	0.4	5×10^{-7}	0.9	0.8
citeseer (0.71)	5×10^{-2}	5×10^{-5}	0.6	1×10^{-5}	0.5	0.2
pubmed (0.79)	1×10^{-2}	5×10^{-2}	0.6	1×10^{-6}	1	0.3

Table 7. Hyperparameters of DGAT on geom datasets

F. Additional Ablation Studies

Table 6 gives the ablation results on the datasets from (Pei et al., 2020). The results suggest that the utilization of three proposed mechanisms, namely topology-guided graph rewiring, global directional attention, and parameterized

Dataset ($H_{\text{node}}(\mathcal{G})$)	GAT [†]	DGN	DGAT
chameleon (0.25)	42.93	50.48 ± 1.26	52.47 ± 1.44
squirrel (0.22)	30.03	37.46 ± 1.28	34.82 ± 1.60
actor (0.22)	28.45	35.47 ± 1.13	35.68 ± 1.20
cornell (0.30)	54.32	77.03 ± 4.72	85.14 ± 5.30
wisconsin (0.16)	49.41	82.75 ± 3.01	84.71 ± 3.59
texas (0.06)	58.38	78.11 ± 4.90	79.46 ± 3.67
cora (0.83)	86.37	84.69 ± 1.32	88.05 ± 1.09
citeseer (0.71)	74.32	73.87 ± 1.32	76.41 ± 1.45
pubmed (0.79)	87.62	84.29 ± 0.61	87.93 ± 0.48

Table 8. Benchmark with baselines on nine small real-world datasets. The best results are highlighted. Results “†” are reported from (Pei et al., 2020). For fair comparison, we use the same experimental setup as (Pei et al., 2020), and report the average test accuracy over the same 10 fixed splits.

normalized Laplacian matrix, enhances the original GAT. Additionally, consistent with the earlier observation, graphs exhibiting stronger heterophily characteristics experience greater benefits from the directional message passing approach. Furthermore, it is worth noting that the use of graph rewiring in DGAT yields remarkable performance enhancements. These improvements contribute to the enhanced performance on the heterophilic datasets, namely *chameleon*, *squirrel*, *actor*, *cornell*, *wisconsin*, and *texas*, resulting in performance gains of 22.22%, 15.95%, 25.41%, 56.74%, 71.44% and 36.11% respectively.